Electrochemical Performance of Carbon Modified $LiNiPO_4$ as Li-Ion Battery Cathode: A Combined Experimental and Theoretical Study

Mehwish Huma Nasir,[1,2,3] Naveed Kauser Janjua,[1,z] and Jay Santoki[3]

[1]*Department of Chemistry, Quaid i Azam University, 45320 Islamabad, Pakistan*
[2]*Institute for Applied Materials (IAM ESS), Karlsruhe Institute of Technology, D 76344 Eggenstein Leopoldshafen, Germany*
[3]*Institute of Applied Materials (IAM CMS), Karlsruhe Institute of Technology (KIT), D 76131 Karlsruhe, Germany*

This study demonstrates the synthesis of olivine $LiNiPO_4$ and carbon modified $LiNiPO_4$ (LNP/C composites) cathode materials for use in lithium ion batteries (LIBs) synthesized via non aqueous sol gel process. The LNP/C composites were fabricated through high energy ball milling of $LiNiPO_4$ with different weight ratios of conductive carbon black. The electrochemical performance of $LiNiPO_4$ has been considerably improved by modifying the material with conductive carbon black which enhanced cathode performance as thoroughly studied by electrochemical analysis. Discharge capacities of LNP/C composite cathodes with 25 wt% carbon were 175 mAh g^{-1}, 150 mAh g^{-1} and 125 mAh g^{-1} with corresponding capacity retention of 82.7%, 84.1% and 82.2% after 100 cycles at 0.05C, 0.1C and 1C rates, respectively. High temperature electrochemical impedance spectra correspond to decreased charge transfer resistance with increased electronic conductivity and minimum cell polarization for the LNP/C powders. Additionally, the inflow of lithium ion flux in cathode particle was simulated by using phase field modeling indicating the coexistence of Li poor and Li rich phases during charging and discharging processes. The findings are significant for the development of optimal battery electrode materials as the methodology and insights used are readily transferable to other ion insertion based electrodes.

Rechargeable lithium ion batteries (LIBs) are considered as one of the significant advance energy storage systems. LIBs have dominated as promising power source option for electric vehicles and electronic devices for possessing long life cycle, high energy densities, safety and environment friendliness.[1,2] In the commercial Li ion cell, mostly cobalt based oxides are used as cathode materials, but its large scale use is prohibited due to high cost.[3] Unique new and improved cathode materials are continuously being developed to cope with the demanding capacity and stability issues in LIBs.[4,5]

In the past few years, extensive studies have been carried out on lithium conducting metal phosphates, $LiMPO_4$ (M = Ni, Mn, Co, Fe) as promising polyanion cathode materials for lithium ion batteries on account of their inherit merits such as good thermal stability, stable potential plateau, decent electrochemical properties, low cost, envir onment benignity and excellent cycling performance.[6,7] Among these olivine phosphates, $LiFePO_4$ as cathode material has been researched in detail and is also well optimized for its use in LIBs as cathode material.[8] However, the drawback related to this material is its low operating voltage at 3.45 V against Li^+/Li, which implies that its energy storage performance is not fully adequate for small and powerful compact LIB devices.[9] Thereby, to overcome these short comings and to enhance the energy densities, research has been focused now on finding alternative to state of the art active materials as $LiCoO_2$ and $LiFePO_4$ cathodes and developing new high voltage cathode materials as per need for a new generation batteries and in purview of rapid growth of electrical vehicle market.[10 13] Substantial attentions have been paid recently on cost effective transition metals as dopants such as Mn, Co and Ni, which produce high voltage plateaus (4.1, 4.7 and 5.1 V, respectively).[14 16]

Among all the olivine phosphates, generation of high voltage Ni based olivine cathodes is of great interest because of high redox potentials (>4.5 V vs Li^+ /Li) and specific energy (800 W h g^{-1}).[8] However, relatively limited research has been done so far on Ni based olivine cathodes because its fundamental features have not yet been thoroughly explored. Therefore, it is important to identify the main issues associated with the synthesis of $LiNiPO_4$ (LNP) nanomaterials as positive electrode and the cycling and electro chemical performances for LIBs.[17]

Another major drawback associated with $LiNiPO_4$ as cathode materials is the low electronic and ionic conductivity due to poor Li^+ intercalation/deintercalation kinetics.[18] It is expected that enhance ment in electronic conductivities can improve charge and discharge performances of $LiNiPO_4$ cathodes.[5,19] Carbon modification has been proved to be an effective methodology to improve the ionic and electronic conductivities of LIB cathode materials. The presence of carbon can also help to obtain small sized particles via preventing the particle aggregation and grain growth.[20 25] Nanometer sized particles deliver enhanced electrical properties with improved LIB performance due to the increased surface area and reduction of diffusion lengths for lithium ions during the performance.[26,27]

Electrical conductivities of $LiNiPO_4$ together with their compo sites have been studied previously[28 30] and carbon coated samples showed better conductivities as compared to bare $LiNiPO_4$.[30] $LiNiPO_4$ synthesis by Pechini method,[31] and polyol method,[32] while improved electrical conductivities have also been reported upon doping with dopants as Mg^{2+}, Zn^{2+},Cu^{2+} and Al^{3+}.[33,34] Cycling performances were improved by carbon modification of $LiNiPO_4$ synthesized by a combined solvothermal and solid state route.[35 37] Enhanced electrical conductivities were also reported in Zn doped $LiNiPO_4$ as well as high discharge capacities were obtained by Mn doping in $LiNiPO_4$ synthesized by polyol method.[14,38] Mg doped $LiNi_{1-y}Mg_yPO_4$ graphite carbon composites showed better specific capacity.[39]

Herein, the destined synthesis of $LiNiPO_4$ by one pot synthesis route using sol gel method is being reported. For the first time, the effect of calcination environment (either air or argon) on $LiNiPO_4$ crystal structure has been clearly documented, which has a sig nificance subsequent effect on their electrochemical performances. The precursor decomposition was investigated in detail using thermogravimetric analysis. Materials characterization, electroche mical properties and detailed analysis of synthesized $LiNiPO_4$ and its LNP/C composites was carried out. Electrochemical perfor mances and enhanced cycling stability of the prepared composites have been thoroughly investigated using galvanostatic cycling,

[z]E-mail: nkausarjanjua@yahoo.com; nkjanjua@qau.edu.pk

cyclic voltammetry and impedance spectroscopy. The carbon modified LNP/C composites significantly improved the cycling performance. The lithium ion diffusion coefficients were also evaluated using button cell testing.

Another objective of the present work was the investigation of intercalation kinetics of $LiNiPO_4$ particle using simulation studies to emulate a particle in real existence. The phase field modelling was executed using the software package PACE3D. The coexistence of Li poor and Li rich phases during charging and discharging pro cesses in LIBs performance was indicated.

Experimental

Synthesis. Non aqueous sol gel method was used to synthesize olivine orthophosphate, $LiNiPO_4$ and carbon modified $LiNiPO_4$ cathode candidates (LNP/C composites). Generally, the synthesis process consists of heating the gel precursors followed by calcination.[40] Metal acetates of lithium ($LiOOCCH_3$).$2H_2O$, (Alfa Aesar); and nickel, $Ni(OOCCH_3)_2.4H_2O$, (Sigma Aldrich), H_3PO_4, (Sigma Aldrich) and ethylene glycol, (Sigma Aldrich) were used as precursors. A non aqueous solution was prepared by mixing the stoichiometric ratios of metal acetates with ethylene glycol while H_3PO_4) was added dropwise (adjusted to a mole ratio of 1:1:1) under stirring and heating at 200 °C for 2 h. The produced gel precursors were calcined at 450 °C, 550 °C and 650 °C for 12 h in tube furnace under argon atmosphere (and in air) with a heating rate of 1 °C min^{-1} and a dwell time of 12 h and cooled to room temperature with a cooling rate of 0.5 °C min^{-1}. Black and yellow powders were obtained via argon atmosphere and air sintering, respectively.

Mechanical milling. Mechanical milling was performed for carbon modification, the calcined powders were further treated by dry grinding step in a planetary ball mill (Pulverisette5, Frisch) using yttria stabilized zirconia beads (100 g, 3 mm diameter). Individual calcined powders were dry ball milled in 80 ml milling chamber with conductive carbon (Super C65, Timcal) and binder (PVDF) in respective ratios of 82:15:3 and 72:25:3 wt% for 15 and 25 wt% carbon modification. The ball milling was continued for 48 h and the obtained powders were LNP/C composites.

Chemical and structural characterization. The physical and chemical composition of the synthesized material was analysed by different analytical methods. The morphology of the composites is characterized by scanning electron microscopy (SEM) and measure ments of the specific surface area (A_{BET}). For SEM, a field emission scanning electron microscope (Supra 55.Zeiss) with accelerating voltage of 10 kV was used to obtain micrographs. To obtain A_{BET}, Gemini VII 2390 (Micromeritics) was used and nitrogen physical adsorption isotherms were measured. The calculation was performed in accordance with the Brunauer Emmett Teller (BET) theory.

In order to resolve the crystal structure of the prepared materials, powder X ray diffraction (D5005 diffractometer, Siemens) and Fourier transform infrared spectroscopy (Vertex 70, Bruker) in attenuated total reflectance mode (ATR) were applied. XRD measure ments of as prepared composites were performed with a Sol X detector using Cu kα radiation. XRD patterns were recorded in the range of 15° to 80° with 0.02° step and counting time of 5 s. TOPAS version 4 from Bruker AXS was used for Rietveld refinement. For FTIR analysis a diminutive amount of the sample was pressed in KBr and spectra were obtained as an average of 5 scans using the OPUS Software Package for data acquisition. The pyrolysis of precursor powders was performed by TG/DSC experiments using a STA 449C thermal analyzer (Nietzsche) in argon atmosphere up to temperature of 800 °C with a heating rate of 5 °C min^{-1}. Particle size distribution was measured using laser scanning Horiba LA950. For retrieving the Raman spectra, Horiba Lab RAM HR spectrometer was used.

Preparation of cathode films and electrochemical characterization. The obtained LNP/C composites containing LNP/C, carbon (C Nergy Super C65, Timcal), binder (Solef PVDF 5130/1001, Solvay) with a weight ratio of (72:25:3) and (82:15:3) were dispersed in N Methyl 2 pyrrolidone (NMP). A thin film of slurry of each composite was used to prepare cathode film by blade coating on an aluminium foil current collector followed by drying under vacuum for 24 h. Swagelok type cells were used for electrochemical measurements. Assembling of cells was done in argon filled glove box in which water and oxygen contents were maintained less than 1 ppm. The cell consisted of prepared cathode film (active mass loading: 2 3 mg cm^{-2}), lithium anode with a glass fibre separator (Whatman GF/C) and 120 μl electrolyte consisting of ethylene carbonate dimethylene carbonate (EC:DMC) at a ratio of 1:1 and 1 M LiTFSi. Galvanostatic charge/discharge technique was used to execute electrochemical measurements using a battery cycler (BT 2000, Arbin instruments). Cells were cycled at a constant room temperature between a voltage window of 4.6 5.7 V (vs Li/Li^+) at a constant current constant voltage protocol at different charge and discharge rates.

For high temperature impedance measurements, three layered asymmetrical cells were pressed by uniaxial pressure with a load of 80 MPa in an order: LNP/C composites as cathode, GDC (gadoli nium doped ceria) as electrolyte and NiO as anode. Asymmetrical cells (cathode/electrolyte/anode) with the diameter of 20 mm with silver coated on both sides (as current collector) were operated at temperatures ranging from 700 °C to 900 °C at 50 °C intervals and their EIS spectra were investigated in detail. EIS measurements were performed on asymmetrical cells under open circuit conditions in 1 MHz to 100 mHz range.

Results and Discussion

In the following sections, the materials synthesis, characteriza tion and electrochemical performances are presented. To ensure high quality single phase LNP/C composites, thorough material characterization was carried out prior to the electrochemical investigation. Different electrochemical cells were used to test the materials in order to focus on both the electrode engineering aspects and material properties. Electrochemical tests were firstly performed on Swagelok cells loaded with $LiNiPO_4$ powders mixed with conductive agent to focus entirely on active material. The impact of different diffusion processes, source of electrode resistance and the origin of enhanced electrochemical performance of carbon modified LNP/C composites was then identified.

To ensure smooth narration, $LiNiPO_4$ (LNP) samples synthesized under various conditions were coded as: LNP/A synthesized in air, LNP/Ar for argon, LNP 823 C15 for LNP synthesized at 550 °C and ball milled with 15% carbon, LNPC 923 C15 for LNP sintered at 650 °C and ball milled with 15% carbon and LNP 923 C25 sintered at 650 °C and ball milled with 25% carbon.

TGA-DSC and FTIR analysis. The prepared composites were identified quantitatively by thermogravimetric analysis and qualita tively by vibrational spectroscopy.

Thermal gravimetric analysis (TGA) was carried out to determine the decomposition temperature and thermal stability of the prepared LNPs,.[41] LNP gel precursors at the heating rate of 1 °C min^{-1} and cooling rate of 0.5 °C min^{-1} over the temperature range of 0 °C to 800 °C were thermally analysed in air and argon atmospheres (Figs. 1a and 1b). For LNP/A, two major weight loss zones, one in 161 °C 219 °C range and other in the 219 °C 371 °C in decomposition temperature profile were detected and associated to organic matrix decomposition. With respect to DSC scans, the organic matrix decomposition leads to two well defined thermal transitions. A first endothermic transition is related to evaporation of residual water and second exothermic peak is due to oxidation of organic matter including acetates. The whole sintering process can be divided into three stages; in the first step as the temperature is increased to around 219 °C, the dramatic mass loss up to 11% is mainly due to evaporation of moisture in gel as well as

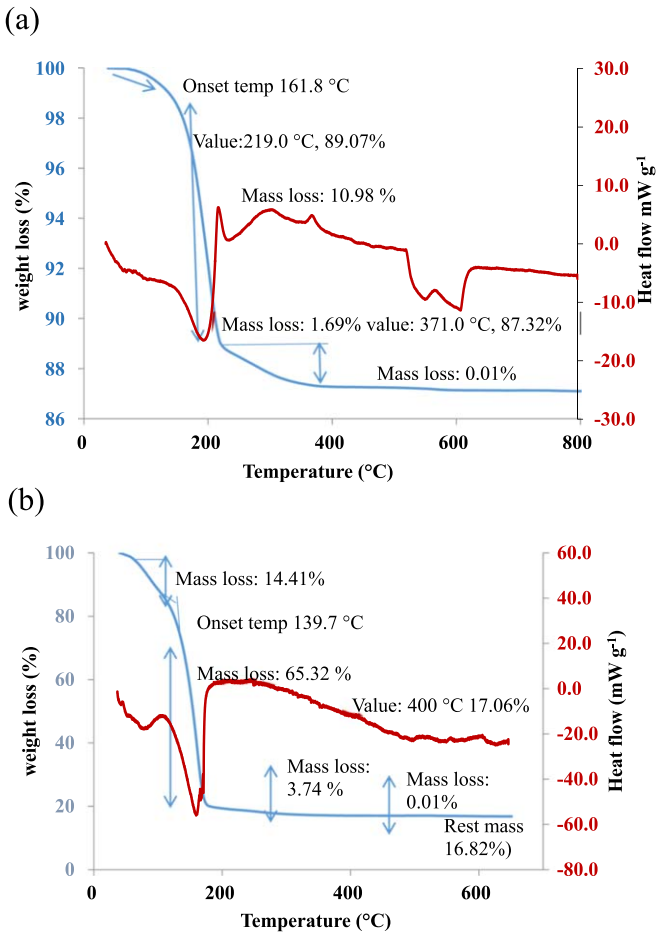

Figure 1. TG DSC of decomposition of LNP gel precursors under air (a) and argon (b) at heating rate of 1 °C min ^{1}.

decomposition of organic matrix which resulted from Li , Ni acetate complexes. In the second step up to 371 °C, mass loss continues but much less significantly, which is associated with remaining organic matrix in the gel, while in last step above 500 °C, the mass of reactants was maintained at 87.32% of initial mass, suggesting that no more mass loss occurred and $LiNiPO_4$ powders started to crystallize.

For LNP/Ar, a significant mass loss of 65.32% was observed when temperature was increased up to 200 °C. Afterwards, no further significant mass loss was observed as the gel stabilized. DTG thermogram revealed a sharp peak at 163.06 °C indicating rapid decomposition of nickel acetate.[5] A constant weight after 200 °C indicated that no heat is used for evaporation and decomposition processes and that $LiNiPO_4$ can be obtained by firing the precursor at temperature above 200 °C. Based on thermogravimetric results, three temperatures were selected; 450 °C, 550 °C and 650 °C as point of interest for the production of $LiNiPO_4$ via calcination of gel precursors.

Similarly, TGA analysis was also carried out for the LNP 823 C15, LNPC 923 C15, and LNP 923 C25 samples before and after ball milling with carbon black. TGA curve of LNP/Ar and LNP 923 C25 (Figs. 2a and 2b) showed initial weight loss up to 180 °C due to the removal of moisture contents while from (200 °C 400 °C) the weight loss is due to the decomposition of gel precursors from in situ formed meta stable complex. That is the decomposition of phos phoric acid and ethylene glycol to release CO_2 and NH_3 followed by the final decomposition of chelated metal complex were observed by exothermic peak at 462 °C in DTA curve. The pristine compound formation started at around 450 °C and completed at ∼600 °C with no further significant mass loss after 600 °C.

The FTIR vibrational spectra of the LNP/C composites are shown in Fig. S1 (available online at stacks.iop.org/JES/167/130526/mmedia) and the presence of various functional groups is confirmed.[42 44] The four fundamental $(PO_4)^{3-}$ vibrations include, a singlet around ν 971 cm^{-1}, assigned to asymmetric stretching of P O bond; a doublet around ν 472 cm^{-1} assigned to symmetric bending of O P O bond and two triply generate $\nu 3$ and $\nu 4$ modes at 1057 1149 and 582 648 cm^{-1}, respectively. Additionally, the peak observed at 546 cm^{-1} may be ascribed to asymmetric stretching vibration of Ni O bonds in NiO_6 octahedra. The band at 472 cm^{-1} is suggested to originate from Li^+ ion translations. These observations confirmed the presence of main functional groups related to Ni and phosphate ions. The C C stretching vibrations in FTIR spectra of the LNP 923 C15 and LNP 923 C25 samples led to the peak at around 1600 cm^{-1}. Vibrational spectra data and band assignments are listed in Table SI.

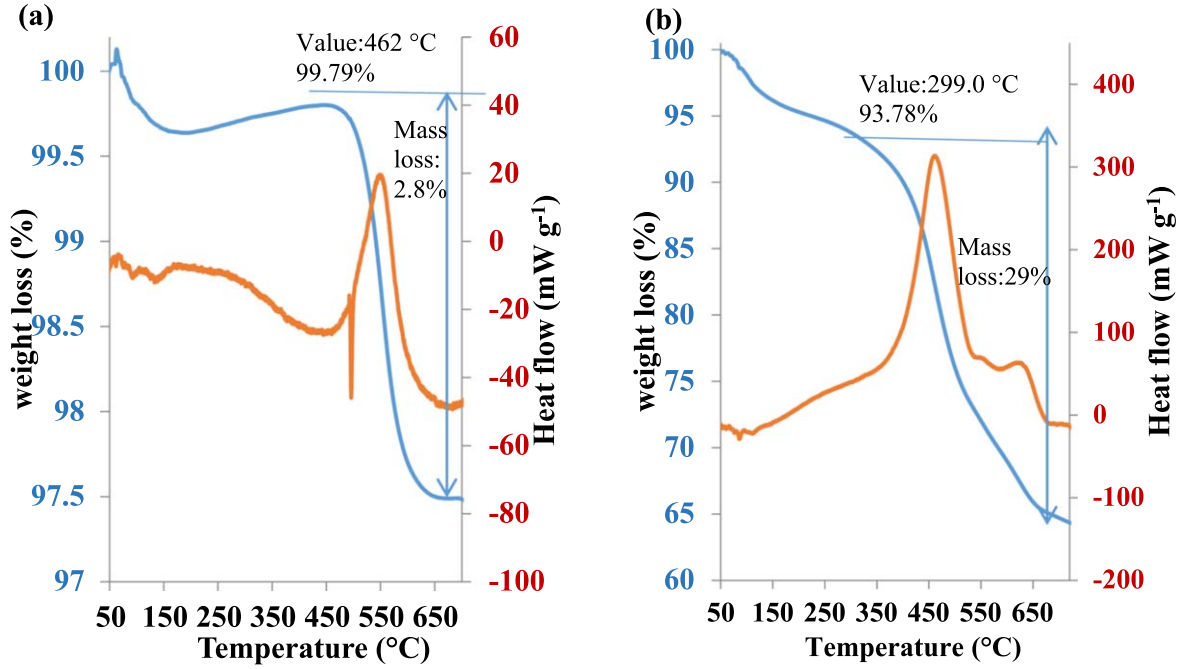

Figure 2. TGA DSC curves of LNP 923 C25 before (a) and after ball milling with 25% carbon (b).

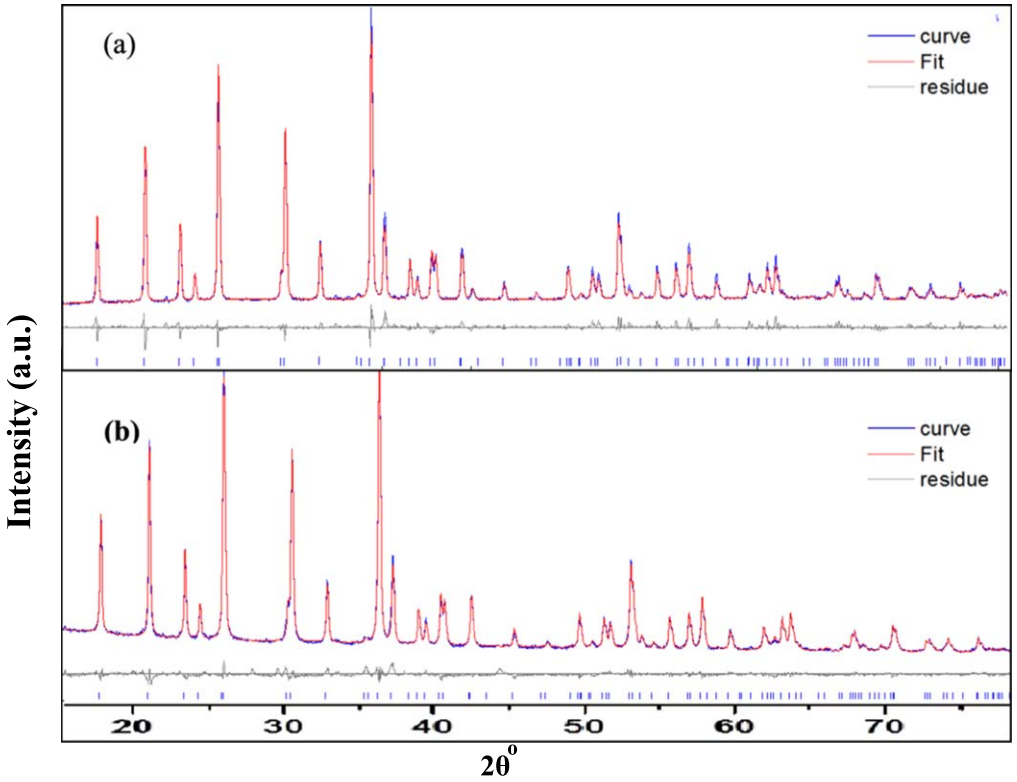

Figure 3. Rietveld refinement of LNP/A (a) and LNP/Ar powders (b).

Structural and morphological characterization. The crystal structure of the compositions was studied using XRD. Comparison of the XRD patterns for LNP powders obtained under air and argon atmosphere are shown respectively in Figs. 3a and 3b. The thermodynamic stable modification of $LiNiPO_4$ is the orthorhombic form. Rietveld refinement was used to refined XRD data of synthesized and ball milled samples in order to obtain a detailed crystal model. Refinement confirmed the orthorhombic structure of LNP with *Pnma* space group. Crystallite sizes obtained for LNP/Ar was smaller than LNP/A. No peak was found for carbon which indicated the presence of amorphous carbon. LNP formed was highly crystalline and pure as no impurity (Li_3PO_4) peak was found (except a small peak at 42.5°) in LNP/A powder prepared under air atmosphere.

XRD patterns of synthesized $LiNiPO_4$ at different temperatures and LNP/carbon/binder composite powders are shown in Fig. S2. All the peaks clearly indicated orthorhombic olivine structure with P*nma* phase group and good agreement with JCPDS No. 81 1528.[35,45,46] Sharpness of peaks is also suggestive of highly crystalline purity. The peaks in ball milled powders exhibited large widths because of the relatively smaller crystallite size which was confirmed by the particle sizes obtained by Rietveld refinement, but positions of peaks were not disturbed indicating the integrity of crystal structure. No carbon peak appeared in the diffraction patterns which is also an indication of the presence of amorphous carbon.

The lattice parameters, cell volumes, densities and crystallite sizes obtained by Rietveld refinement are shown in Table SII. low Rwp values confirmed a good fit of the observed profile. With increase in temperature from 550 °C to 650 °C and by increasing carbon contents, lattice parameters decreased. This could be explained by the fact that at high calcination temperature, more carbon will be oxidized forming CO_2 and thus more room for $LiNiPO_4$ crystal to get organized and cell volume gets smaller.[47] In all the prepared powders, the porosity decreased hence, density increased with increase in temperature (Fig. S3).

For electrochemical applications, the cathode material should be porous as it enables Li ion transport.[48] Morphologies of the samples were analysed by FESEM and the micrographs of the samples are shown in Fig. 4. Particles prepared under argon were much smaller in size than LNP particles obtained under air. The particles possessed clearly distinguishable grain boundaries and smooth surface with nearly equal particle size and shape distribution. LNP 923 C15 and LNP 923 C25 samples presented the particle sizes with a ca. 40 84 nm and ca. 40 96 nm.

Particles calcined at 650 °C were less agglomerated and least charging effect could be seen, which indicated the better electro conductive behaviour. Particles are spherical in shape which increases the surface area of the interface. In situ decomposition of ethylene glycol forms a thin carbon layer on the surface of particles which can greatly improve the electrical contact between the particles.[49] As a result of which, electrolyte can help penetrate active substance to enable the transportation of electrons and Li ions and resultantly, improve the utilizations of LNP/C composites.

Further, the elemental compositions of LNP/C composites were elucidated by SEM/EDS as collected in Table SIII. The obtained elemental concentration ratios are very close to the expected concentrations thus conforming to the right synthesis route.

The calcination process is expected to generate agglomerates of primary particles; thus, the powders were ultra sonicated in iso propanol for 15 min and the particle size was determined using laser scattering analysis (LSA). Results of particle size analysis are shown in Fig. 5a. Distribution of primary particles broadens with consistent decrease in bimodal distribution for the samples which are ball milled with carbon.

The Brunauer Emmett Teller (BET) surface area of LNP/C composites was determined by N_2 adsorption isotherm. These isotherms can be characterized as a Type II which is suggestive of the presence of micropores (Fig. 5b).[50] The measured surface areas for LNP/Ar was 35.94 $m^2\ g^{-1}$ which was increased to 87.16 and 94.79 $m^2\ g^{-1}$ for LNP 923 C15 and LNP 923 C25, respectively, which can lead to more contact between active material surface and electrolyte that facilitates the electrochemical reactions. The d_{BET} was calculated from specific area is 0.017 μm and 0.016 μm for LNP 923 C15 and LNP 923 C25, respectively ($d_{BET} = 6/(\rho\ A_{BET})$

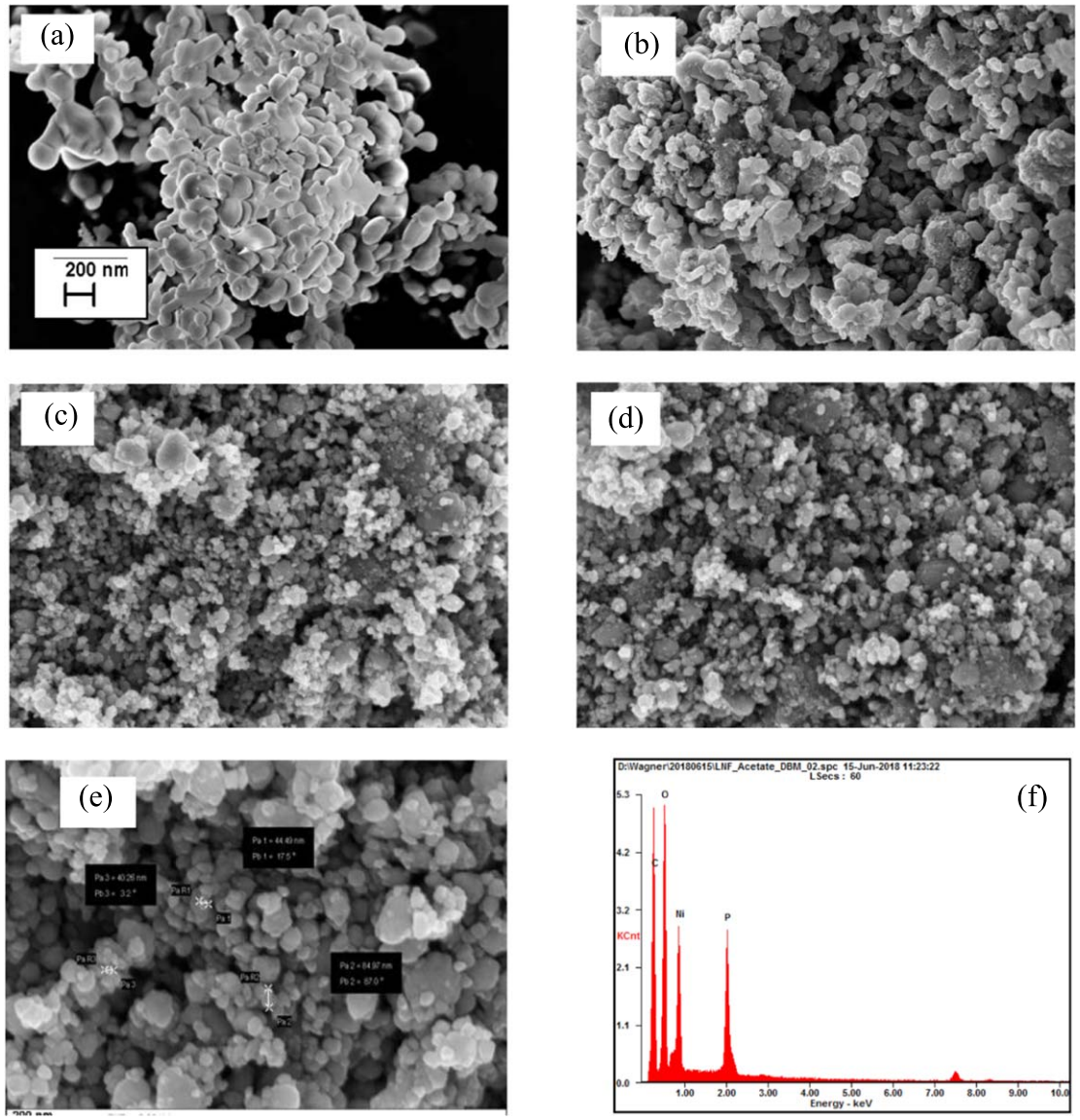

Figure 4. SEM images of LNP/A (a) LNP/Ar (b) LNP 923 C15 (c) LNP 923 C25 (d) LNP 923 C25 (high magnification) (e) EDX spectra of LNP 923 C 25 (f).

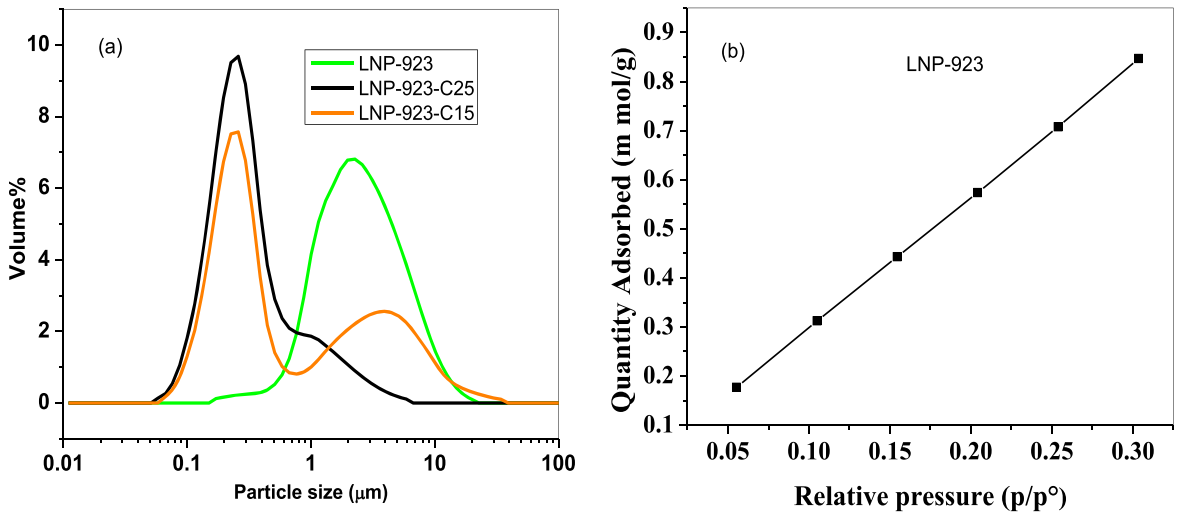

Figure 5. Particle size distribution of LNP/C composites (a) N_2 adsorption isotherm of LNP 923 (b).

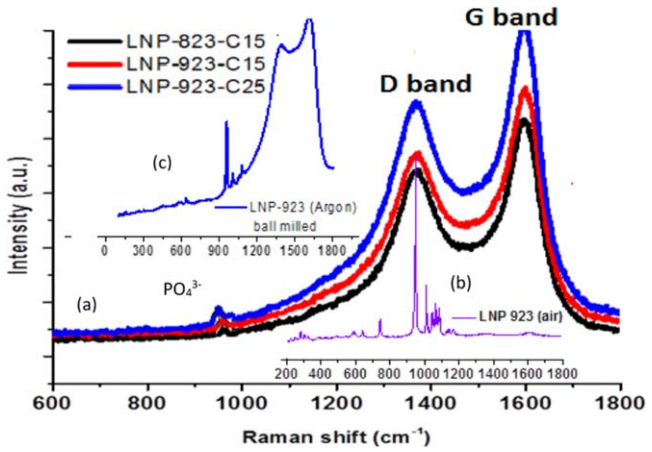

Figure 6. Raman spectra of LNP/C composites; LNP 823 C15, LNP 923 C15 and LNP 923 C25 (a) LNP/A (b) LNP/Ar (c).

10^{-6} in m, ρ is attained from Rietveld refinement).[51] Somewhat larger d_{BET} values compared to the values derived from SEM micrographs are due to particle aggregation and reduced surface areas. The values are shown in Table SIV.

Further, in order to characterize the detailed bonding structure of LNP/C composite, Raman spectroscopy is carried out. Raman spectra (Fig. 6) clearly displayed the characteristics vibrational modes of $LiNiPO_4$. Carbon modification enhanced the Raman activity to several orders of magnitude compared to that of LNP/A and LNP/Ar. Spectra of LNP/C composites are shown in Fig. 6a in which the peaks in the range of 1250 1450 cm^{-1} and 1550 1660 cm^{-1} are assigned to the disorder induced phonon mode (D band, sp^3 character carbon) and graphite band (G band, sp^2 character carbon), respectively. I_D/I_G ratio determines the quality of carbon and degree of deformation in carbon matrix. Lower I_D/I_G ratio values show smaller deformation and more graphitization i.e., more ordered composites.[40] It was perceived that extent of deformation decreased with ball milling which was calculated by I_D/I_G ratio of the LNP/C composites. The values are 0.857 for LNP 823 C15, 0.853 for LNP 923 C15 and 0.848 for LNP 923 C25, which demonstrates that the quality of sp^2 character carbon is much greater than sp^3 character. Presence of carbon with much sp^2 characters is advantageous to the electronic conductivity and enables the facile diffusion of Li^+ ion. Thus, the carbon modification under optimised conditions, can help improve the cathode activity.

Resultantly, it is supposed that the reduced crystallite size and lower crystallinity of LNP/C composites obtained after ball milling and addition of carbon leads to high specific surface area. These parametric observations may in turn shorten the diffusion paths for Li ions to be inserted between the phosphate layers. This will surely help to achieve higher specific discharge capacities and excellent cycle stability in the electrochemical performance of the envisioned cathode material.

Electrochemical performances. To explore the electrochemical performances, Swagelok cells were assembled (as described in experimental part) which were examined using galvanostatic cycling and charge and discharge plateaus were recorded. Tests were performed in the voltage window of 4.6 5.7 V using 1 M lithium bis (trifluoromethanesulfonyl)imide in ethylene carbonate: dimethyl carbonate (1:1 vol.%) (1 M LiTFSi (EC:DMC; 1:1 vol%)) as an electrolyte. As the redox couple of $LiNiPO_4$ is expected to show up above 5 V, therefore, the electrolyte is carefully chosen. Lithium imide salts when used in combination with the electrolyte improve the cycling stability and coulombic efficiency. 1 M LiTFSi is used in many high voltage lithium ion batteries which operate at voltage above 5 V. It has the ability of very low volatility as compared to the conventional organic electrolytes which allows it for cycling vs lithium metal anodes. The long cycle stability and presence of less decomposition products make this electrolyte stable even at high voltages (well above 5 V). Altogether, due to inherit physical stability, LiTFSi is proven to be electrochemically stable at high operating voltages. Herein, 1 M LiTFSi (EC:DMC; 1:1 vol%)) has shown excellent stability without any decomposition after cycling it to a voltage of 5.6 V. In the following sections, the electrochemical performances are discussed.[45,52 55]

Figure 7a shows the charge and discharge curves of LNP 923 C15 electrode at 0.1 C rate. Capacities were checked for 100 cycles and are shown in Fig. 7a. The presence of flat plateau at 100th cycle indicates good electrochemical reversibility of the redox couples, Ni^{2+}/Ni^{3+} and Ni^{3+}/Ni^{4+}. Two charge discharge plateaus were obtained, and both contribute almost equal to discharge capacities. First charge and discharge capacities were 160 and 137 mAh g^{-1} at 0.1 C rate. Charge capacity of 115 mAh g^{-1} was obtained at the end of 56th cycle and it was stable up to 100th cycle. With an increase in the cycle number, a slight decrease in the reversible capacity was observed.

Cyclic voltammogram (CV) of the same electrode assembly (Fig. 7b) further confirms the electrochemical activity. Two pairs of peaks in corresponding CV profile were observed which complement the presence of two discharge charge plateaus, one in 5.23 5.27 V and other around 4.93 4.94 V potential ranges which were attributed to oxidation and reduction peaks of Ni^{2+}/Ni^{3+} and Ni^{3+}/Ni^{4+} redox couples (the major contributors towards battery performance).[56] The sharpness and symmetry of redox peaks indicate that kinetics of Li^+ intercalation and deintercalation greatly upgraded. Ni^{2+} ions could not only be oxidized to Ni^{3+} corresponding to one Li^+ intercalation/deintercalation but also partially to Ni^{4+} leading to more than one Li^+ intercalation/deintercalation.[57] After a few cycles, the decreased capacity suggests that the contribution of Ni^{3+}/Ni^{4+} redox couple towards discharge capacity becomes insignificant due to the irreversible interconversion. Figure 7c shows the discharge capacities at different current density rates. The stretch of voltage plateau is observed to decrease with increase in current density. Discharge capacities of 110 and 80 mAh g^{-1} (which is 65% 47% of theoretical capacity of $LiNiPO_4$ cathode material) were obtained at the current densities of 499 and 833 mA g^{-1}, respectively.

The perceived electrode reversibility was 92%, 90% and 88% for 0.05, 0.1 and 1 C rate, respectively. With continuous cycling of LNP 923 C15 Swagelok cell at 0.1 C rate, the discharge capacity is slowly decreased, and it finally delivers discharge capacity of 110 mAh g^{-1} on 100th cycle (Fig. 7a). During the continuous cycling, solid electrolyte layer is formed on electrode electrolyte interface which may cause the resultant capacity fade. The cross section of electrode in which channels are present possesses hair like cracks which act as ionic highways (Fig. 7d). Cycle life performance at different current rates from 0.05C to 5C is represented in Fig. 7e. The impressive cycling performance and superior rate of this electrode should be credited to high degree of crystallization of $LiNiPO_4$ phase which is due to temperature controlled synthesis and nanoscale production by ball milling.

Figure 8a displays the charge and discharge curves of LNP 923 C25 electrode at 0.1 C rate. Similarly, capacities were checked for 100 cycles. Reversibility of redox couple by the presence of flat plateau even at 100th cycle specifies the excellent electrochemical reversibility of the redox couple. First charge and discharge capacities were 192 and 150 mAh g^{-1}. With an increase in the cycle number, there was a decrease in the reversible capacity. Charge capacities of 139 mAh g^{-1} at the end of 26 cycles and 119 mAh g^{-1} at the end of 59 cycles were observed that were stable up to 100 cycles. For LNP 923 C25, continuous cycling of Swagelok cell at 0.1 C rate resulted in slow decrease of discharge capacity and finally, discharge capacity of 120 mAh g^{-1} was delivered with maximum efficiency of 91% in 100th cycle (Fig. 8a).

Two pair of oxidation and reduction peaks vs Li^+/Li in corresponding CV profile was also obtained (Fig. 8b) for

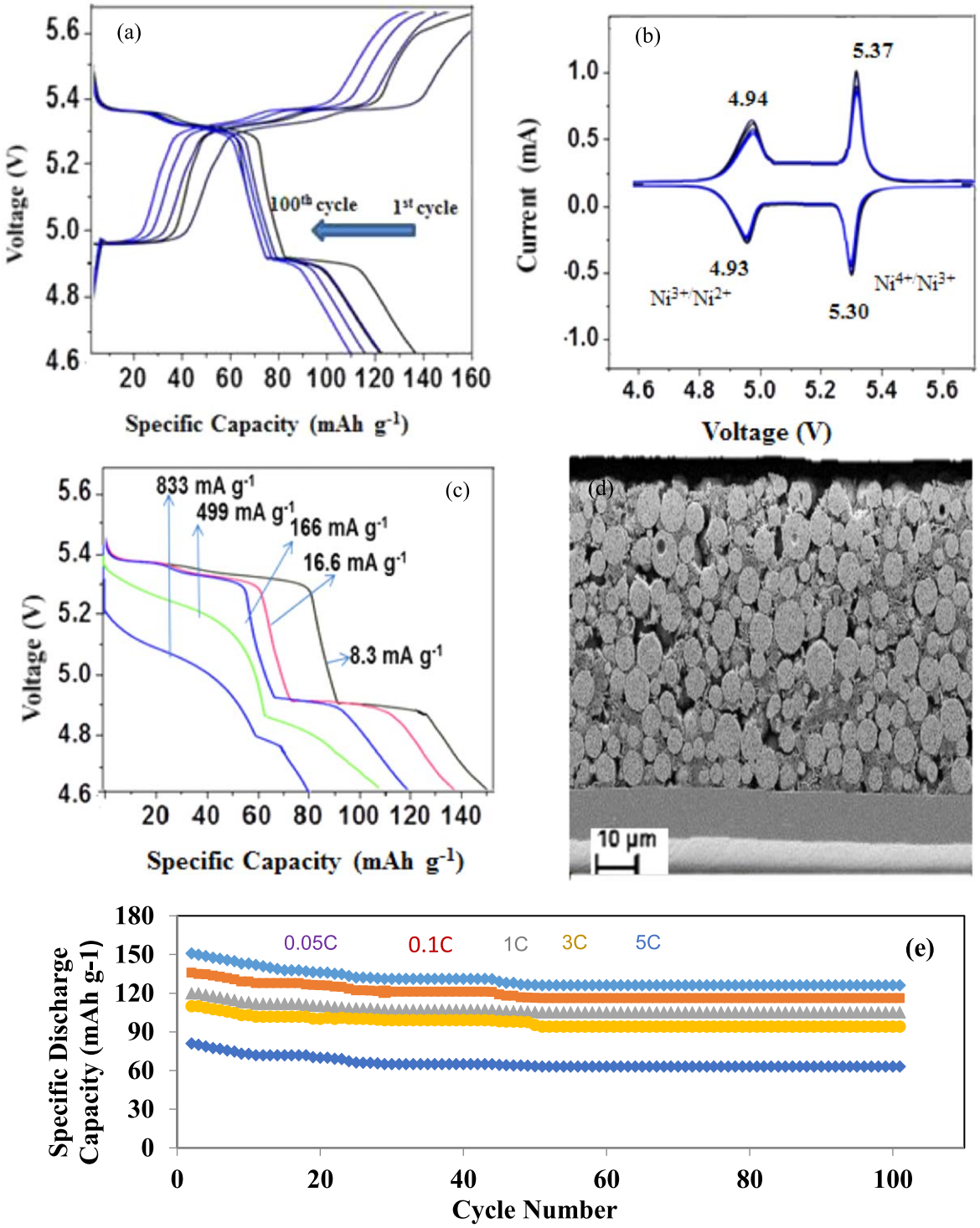

Figure 7. The 1st, 29th, 56th, and 100th discharge curves of the LNP 923 C15 electrode at 0.1 C rate (a) cyclic voltammogram at 1 mv s ^{1} scan rate (b) Discharge capacities at current densities of 8.3, 16.6, 166, 499 and 833 mA g ^{1} (c) Cross section of electrode(d) Cycle life performances of LNP 923 C15 at various C rates (e).

LNP 923 C25 complimenting the presence of two charge and discharge plateaus. Figure 8c shows the observed discharge capa cities at different current densities. Discharge capacities of 90 and 70 mAh g^{-1} were obtained for respective current densities of 499 and 833 mA g $^{-1}$. The apparent electrode reversibility was 93%, 91% and 89% for 0.05, 0.1 and 1 C rate, respectively. These observations are coherent with the earlier reported results. LNP 923 C25 exhibits highest discharge capacity (180 mAh g^{-1}) thus, suggesting that LNP 923 C25 in combination with Li anode would be an excellent alternative for high voltage LIBs. Channels for ionic highways are also observed in cross section of LNP 923 C25 electrode (Fig. 8d). It is evident from SEM micrographs of the cross section of electrode that the LNP/C composite electrodes contain channels which improve the electronic or ionic mobility and therefore, improve the reversible capacity. Cycle life performance at different current rates from 0.05C to 5C is represented in Fig. 8e.

Uninterrupted rate performance of the fabricated cells compar ison at different C rates is shown in Fig. 9. Capacity fades at higher

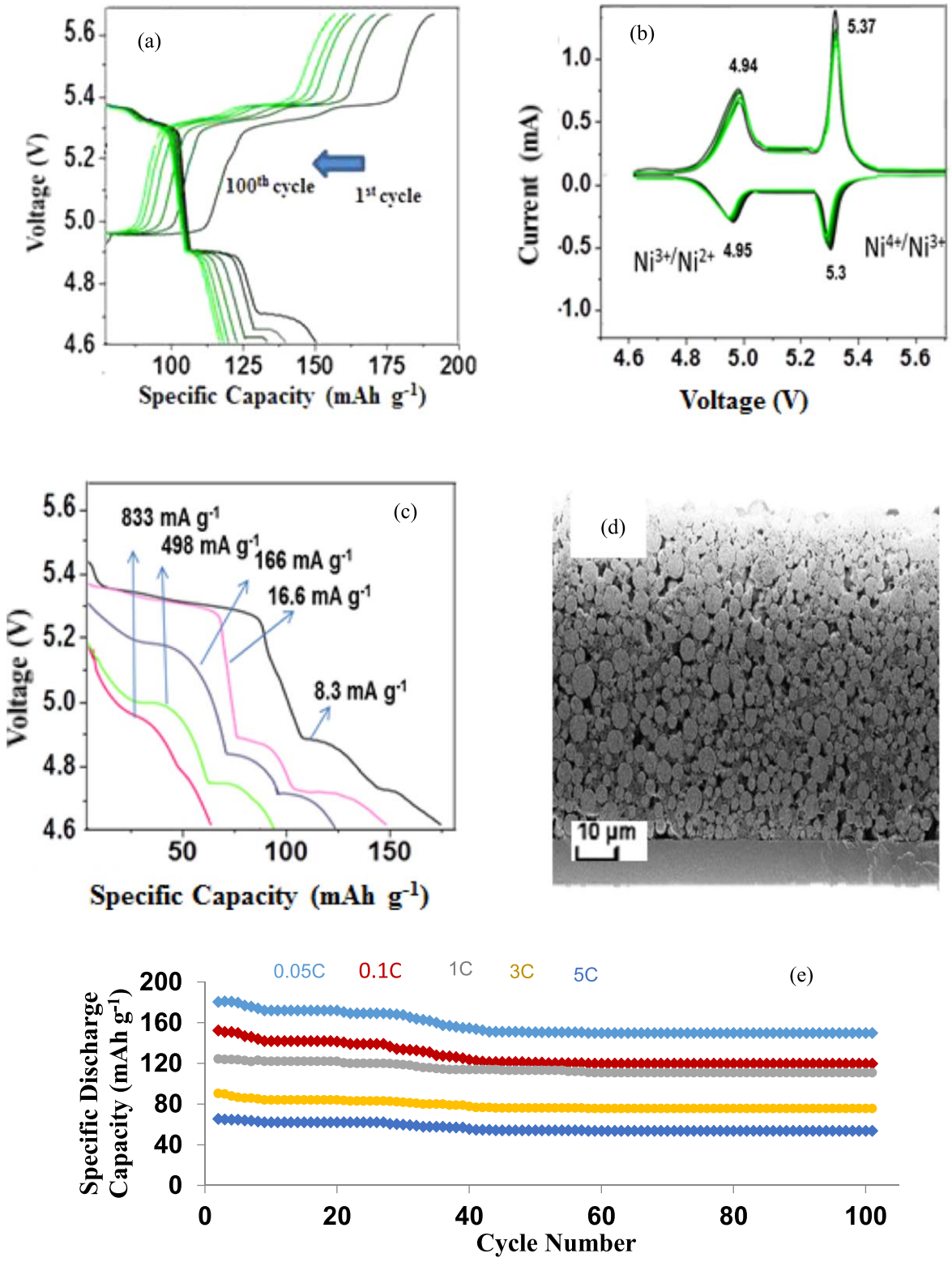

Figure 8. The 1st, 29th, 56th, and 100th discharge curves of the LNP 923 C25 electrode at 0.1 C rate (a) cyclic voltammogram at 1 mv s ^{1} scan rate (b) Discharge capacities at current densities of 8.3, 16.6, 166, 499 and 833 mA g ^{1} (c) Cross section of electrode(d) Cycle life performances of LNP 923 C25 at various C rates (e).

discharge capacities were decided to improve the internal resistance of the electrode.[58] The cells were able to produce the same discharge capacities (C/2 rate) even after cycling at higher C rates. The perceived top rate performance in terms of electrochemical proper ties of produced cathode composites by one pot sol gel and milling with carbon can be due to many factors including improved ionic/ electronic conductivity, high crystallization, high surface charges, small crystallite sizes, reduced charge transfer resistance and high thermal stability.[59] Comparison of the specific discharge capacities at different C rates of the tested cells is shown in Fig. S4. The discharge values of LNP 923 C25 electrode were higher than those of the other electrodes at various C rates which proved the superior

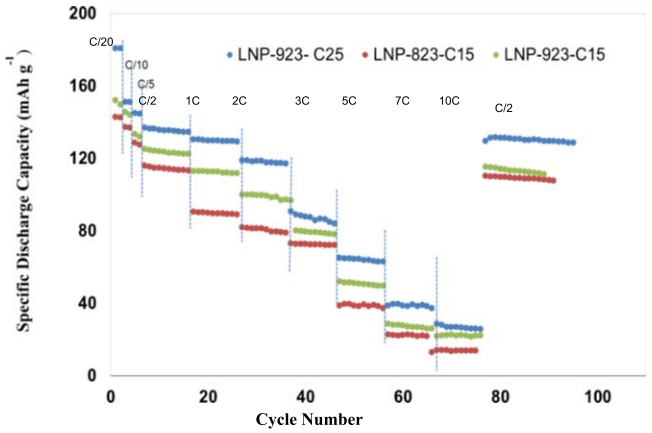

Figure 9. Comparison of uninterrupted rate performance of the LNP/C composite cells at various C rates.

rate performance of this cathode material. Discharge capacities values of LIBs using LNP/C composite cathodes are presented in Table SV.

The presence of two plateaus is not only obtained using galvanostatic cycling but also by cyclic voltammetry. Nickel ions could not only be transformed from Ni^{2+} to Ni^{3+}(corresponding to one Li^{+} intercalation/deintercalation), but also partially to Ni^{4+}, leading to more than one Li^{+} intercalation/ deintercalation. Ni initially proceeds via the oxidation of Ni^{2+} to Ni^{3+}, followed by the oxidation of Ni^{3+} to Ni^{4+}. The replacement of Ni^{3+} by Li^{+} in nickel rich layers is compensated for by the appearance of Ni^{4+} ions. The $LiNiPO_4$ materials exhibit low intrinsic electrical conductivity. Experimental conditions during synthesis and carbon coating significantly improve Li + intercalation/Deintercalation kinetics. Taking advantage of multivalency of nickel ions, an additional lithium ion insertion reaction vs Li^0/Li^+ has been observed. The better kinetics was observed by characterization techniques including XRD, Raman spectroscopy and TGA. Speculation of Ni^{2+}/Ni^{3+} and Ni^{3+}/Ni^{4+} above 4.7 V has also been reported by other research groups previously.[57,60]

In order to evaluate the structural stability of the LNP/C composites, the cells were stopped at discharging state and dismounted. Electrode was rinsed with dimethyl carbonate in order to remove residual electrolyte salt and dried in glove box. Later, the powder was investigated by ex situ XRD (Fig. S5 and S6) and unit cell parameters were refined by rietveld refinement. No impurity peak was found and LNP structure was intact which proved the stability and the change in cell parameter values depict the successful intercalation and deintercalation of lithium ions.

High temperature EIS measurement. Cathode performance of LNP/C composites was tested in asymmetrical cells (LNP ASC) using a three electrode setup. The performance of cells was characterized by electrical impedance spectroscopy as it gives valuable insight into the system. Cole Cole (Nyquist) plots were analyzed to retrieve the impedance data fitted by the equivalent circuit modelling. Three layered asymmetrical cells with LNP 923 C25 as cathode, GDC as electrolyte and NiO as anode were silver coated on both sides and operated at different temperatures and their EIS spectra were retrieved. Figure 10a shows the Cole Cole impedance spectra of asymmetrical cell at temperature ranging from 700 °C to 900 °C at 50 °C intervals. EIS measurements were performed where negative temperature coefficient of resistance behaviour was observed as the increased impedance trends were recorded with decrease in temperature.[61]

Simulated curves and corresponding equivalent circuits which were used to model the electrochemical process for lithium intercalation is shown in Fig. 10b where R represents resistance and CPE stands for constant phase element. In the temperature interval 700 °C 900 °C, incipient arc and second depressed semicircle arc spanning the whole frequency range were obtained. The arcs take the shape of semicircle at lower temperature which decreased as temperature increased indicating good conduction. Below 800 °C, impedance plots consist of depressed semicircles with nonzero intercept. Upon increasing temperature nonzero intercept diminishes. At high temperatures, the electrode reactions are kinetically fast, therefore, fast Li ion intercalation may take place which may lead to low resistance and high conductivity while at lower temperatures due to kinetically slow electrode reactions, a horizontal shift of Nyquist plot along Z′ axis spans indicating an increased resistance trend. In all, as the operating temperature increases from 700 °C to 900 °C, an increase in relaxation frequency of the grain boundary based conduction process occurs and the Nyquist trends shift towards the high frequency region. Therefore, not all arcs are observed at all operating temperatures, with only one semicircle appearing at low temperatures representing the electrode resistance.[62 64]

The intercept at high frequency region (HFR) gives ohmic resistance (R1) that arises from ion conducting resistance of cathode interface with electrolyte The non ohmic part from the EIS curve fitting of data shows two frequency dependent processes at medium (R2 i.e., cathodic resistance) and low frequency (R3 i.e., the anodic resistance).[65] Some of these resistances equals the polarization resistance. It was observed that R1 dominates at relatively lower

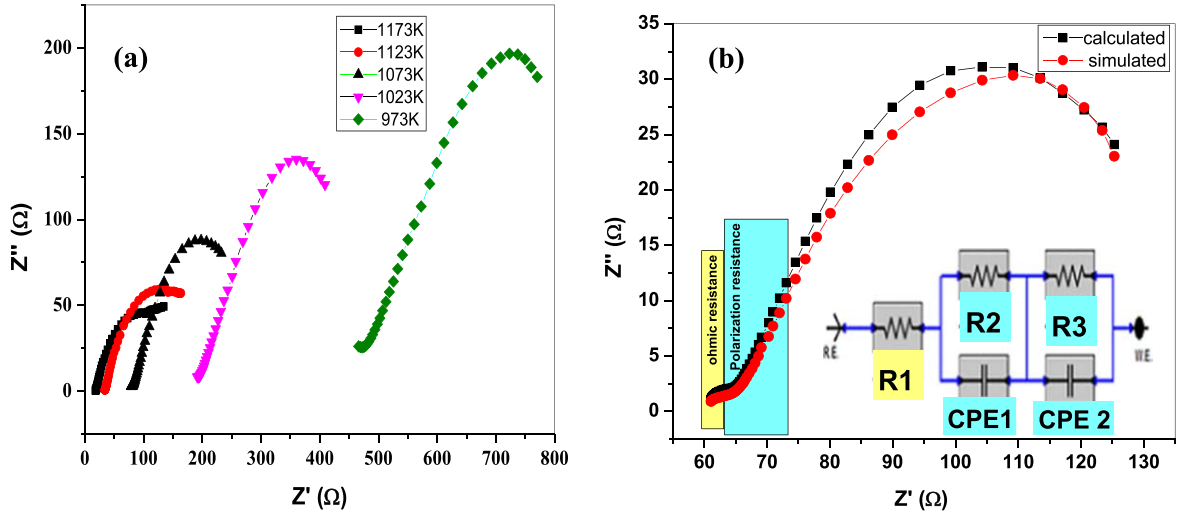

Figure 10. Nyquist plot of LNP 923 C25 at different temperatures (a) Simulated curve and equivalent circuit (b).

Table I. EIS parameters for activation energy using LNP-923-C25 as cathode.

Temperature (°C)	Resistance Rct (Ω)	Resistivity ρ (Ωm)	Conductivity б (Ω ^{1}m ^{1})	log б	1000/T (K ^{1})
700	800.0	55.84	0.0179	1.74	1.02
750	241.7	16.87	0.0592	1.22	0.97
800	180.0	12.56	0.0795	1.09	0.93
850	45.0	3.13	0.3183	0.497	0.89
900	27.1	1.89	0.5274	0.277	0.85

Table II. Corresponding energy of activation and diffusion coefficient.

Cathode Material	E_a /(eV)	D_{Li}^+ (10^{13} cm^2 s ^{1})	
		973 K	1173 K
LNP 923 C25	0.39	7.47	13.91
LNP 923 C15	0.47	3.83	8.48
LNP 823 C15	0.54	1.82	7.72
LNP 923	0.79	0.80	6.47

Table III. Material properties of LNP cathodic intercalation material.

Parameter	Symbol	Value	Unit
Diffusion coefficient	D_o	7.478×10^{13}	m ^{2} s ^{1}
Maximum concentration	C_{max}	22900	Mol m ^{2}
Gradient energy coefficient	K	7×10^{18}	m^2
Regular solution parameter	α_1	2.5	
	α_2	5.2	
Temperature	T_{ref}	300	K

temperatures (700 °C 750 °C) while R2 and R3 becomes more dominant at higher temperatures (800 °C 900 °C) which suggests that diffusion processes at cathode and anode surfaces become more facile with rise in temperatures. The EIS curve showed a depressed semicircle in the HFR that corresponds to charge transfer process of Li^+ intercalation. Rct represents the diameter of semicircle corre sponding to charge transfer resistance that is related to Li^+ intercalation process. The same model remains valid for fitting of EIS data obtained at all temperatures.[66]

The extracted values of resistances from the fit data at different temperatures are given in Table I. Results from EIS modelling revealed that by optimizing the component ratio, (carbon:LNP in the present study) homogeneous microstructures in the composite and small crystallite sizes increase the Li^+ ion transportation. Electrical conductivity of LNP/C composites measured by AC impedance with Au as current collector is shown in Fig. S7 in the form of Arrhenius plot (graph between log of conductivity and temperature).[67] Activation energies are calculated by using Eq. 1 and E_a values are shown in Table II. Activation energy values obtained for LNP 923 C25 was 0.39 eV which is lowest value obtained among all the produced composites which is indicative of its fast Li^+ intercalation and hence, better electrochemical performance.

$$\log \sigma = A' - \frac{E_a}{2.303RT} \quad [1]$$

Further, the diffusion coefficients, D, can elaborate the facility of the lithium ion diffusion, D_{Li}^+ in LNP/C composites and could be derived using Eq. 2.[57]

$$D_{Li}^+ = \frac{R^2T^2}{2A^2n^4c^2\sigma^4} \quad [2]$$

where R is gas constant, T is absolute temperature, n is number of electrons per molecule (attending electron transfer reaction), A is surface area of electrode, C is concentration of Li^+ ion in LNP structure and is obtained from slope of straight line by using Eq. 3[57]:

$$Z_{Re} = R_{ct} + \sigma\omega^{-1/2} \quad [3]$$

where Z_{Re} is impedance at high frequency intercept in Nyquist plot and ω is the frequency.

Lithium diffusion coefficient values estimated at 700 °C and 900 °C are given in Table IV. LNP 923 C15 and LNP 923 C25 have 8.48×10^{-13} and 13.91×10^{-13} cm^2 s^{-1} diffusion coefficients values at 900 °C, which are higher than for LNP/Ar. The higher values of D_{Li}^+ in LNP/C composite based cathodes may impact the charge capacities and improve the resultant battery performance, thus realizing a faster commercialization. It could be concluded that reducing particle size (smaller crystalline sizes) and increasing the surface area by carbon modification and ball milling benefit the movement of lithium ions by shortening the diffusion pathways in LNP cathodes. It is also revealed that carbon modification has decreased the energy barrier to overcome the movement of lithium ions hence, the small activation energies were obtained for carbon coated samples.

Modeling of inflow of Li-ion flux in cathode particle. The understanding of physical and chemical processes at electrode for providing high energy density and improved battery life is of scientific interest.[68 70] The selection of anode material, cathode material or electrolyte depends on various characteristics including, discharge rate, battery cycle time, battery life time and operating temperature.[71,72] $LiNiPO_4$ is a proven candidate for cathode material because of its highest energy density and high operating voltage however, capacity fade is the shortcoming.[39] An important source of capacity fade is two phase coexistence. Cahn Hilliard (CH) equation can represent this two phase coexistence i.e., Li rich and Li poor phases (during intercalation). Two phase coexistence can be repre sented by Cahn Hilliard (CH) equation.[73] In the past few years, the phase field model has been extensively used as a simulation tool to imitate various processes in lithium ion batteries.[74,75] In phase field method, a continuous phase parameter also known as order para meter is used to define the whole microstructure evolution. Order parameter transformations works on optimization principles, such as maximization of entropy or minimization of energy.

In the present study, phase field approach is used to simulate phase separation during Li^+ intercalation in LIBs. Simulation study was performed on LNP cathode particle at a lithiation discharging condition, Figure 11. The experimental results revealed that elec trode consists of particles that show shape diversity. In order to obtain the simulated results that are close to experimental particle geometry has been considered. To imitate real particle, intercalation kinetics of irregular shape particle was studied.[76] Lithium ion intercalation into LNP is investigated by introducing a conserved, continuous phase field order parameter of concentration c (x,t). This parameter (ψ) defines the whole microstructure and has constant values in bulk region but varies continuously in between or at interfaces (Fig. 11a). The field order parameter (ψ) takes the value 0

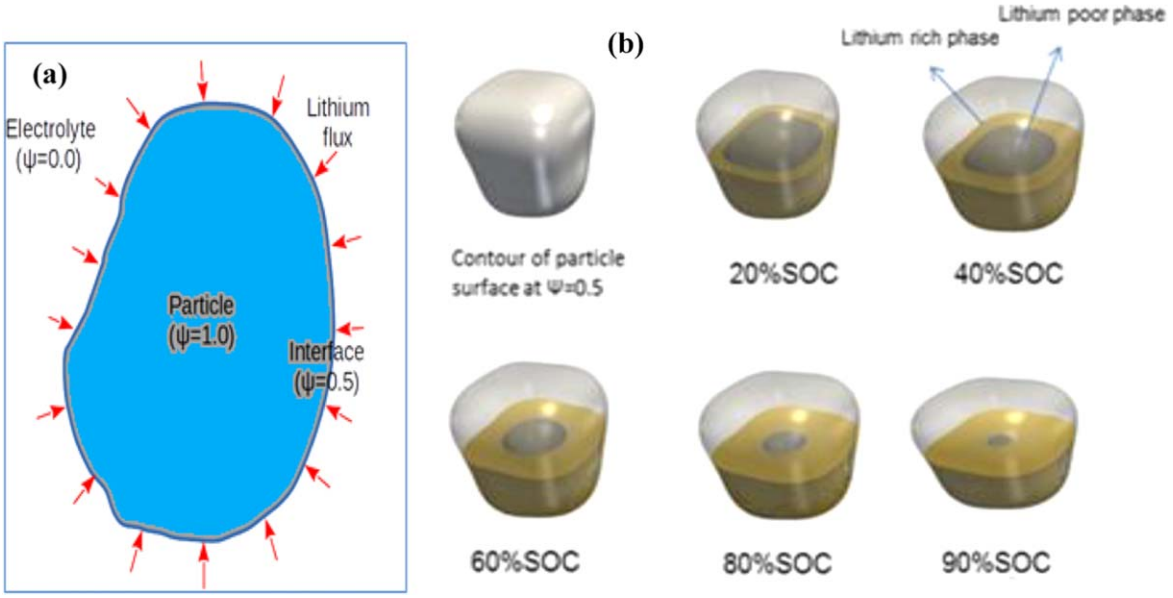

Figure 11. Schematic presentation of a cathode particle surrounded by an electrolyte in LIB (a) Evolution history of an irregular shape 3D particle (b).

Table IV. Comparison of theoretical and experimental discharge capacities attained at different C-rates.

C rate	Discharge capacities (Theoretical) (in %SOC)		Discharge capacities (Experimental) (mAh g ^{1})
	A	B	
0.05	99.88	0.001	175
0.1	98.78	0.002	150
0.2	99.57	0.005	146
0.5	98.71	0.058	139
1.0	85.56	0.108	130
2.0	67.19	0.156	125

for the electrolyte, 1.0 for the bulk cathodic particle and varies smoothly in the boundary (diffuse particle interface) between the particle and the electrolyte. The minimization of system free energy was confirmed by equating the functional derivative to zero.

$$\frac{\partial c}{\partial t} + \nabla \cdot (-M \nabla \mu) = 0 \qquad [4]$$

where c is local lithium ion concentration, M is isotropic lithium ion mobility and μ is chemical potential of system. Table III lists the materials parameter's set for the LNP cathode particle.[73] Diffusion coefficient values obtained experimentally were used for simulation studies. When simulation starts, the inflow of lithium ion flux fills up the particle and at the end, instead of fully lithiated state, simulation stops when c = 0.999. Simulations were performed by varying the aspect ratio of ellipses of equal area.

Figure 11b shows the microstructure evolution (via intercalation) of irregular shape 3D cathode particle to a 20%, 40%, 60%, 80% and 90% state of charge (SOC). The particle was clipped from upper section for better visual sighting. The gold and grey colors correlate to Li rich and Li poor phases, respectively. Phase segregation starts from the surface of the particle where lithium ion flux is applied.

Figure 12a shows the simulation results of five particles with aspect ratio (γ) of 1, 2, 3, 4 and 5 immersed in electrolyte simultaneously. Figures 12b and 12c show the SOC at which phase separation ends. These SOC values correspond to discharge capacities expected at different C rates. The comparison of discharge capacities obtained theoretically by phase field modeling and discharge capa cities obtained experimentally are tabulated in Table IV. The discharge capacities were estimated by finding coefficients of fitted curves, A and B of the plot presented in Fig. 12. The values obtained showed the same trends theoretically and experimentally.

Conclusions

Sol gel method was successfully adopted for synthesis of single phase LNP nanoparticles at temperatures 450 °C 650 °C under argon atmosphere. The processing under argon atmosphere incorpo rated 3% C in LNP. The prepared LNP nanoparticles were processed through in situ carbon modification using high energy ball milling with carbon black as carbon source. Ball milling with carbon black resulted in increased surface area and smaller crystalline sizes. All the LNP/C composites, ball milled with carbon black retained their microstructure and no impurity peak was found in ex situ XRD patterns. Galvanostatic cycling was carried out using LNP/C composites as cathode candidates in LIBs. Carbon modified LNP/C composites prepared by ball milling with 15 wt% and 25 wt% carbon exhibited discharge capacities of 150 mAh g^{-1} and 175 mAh g^{-1} respectively at 0.05C in LIBs. The LNP/C composites exhibited high redox intensity peaks which confirmed fast lithium ion diffusion and hence, improved electrode reduction reversibility inside the host lattice. Modification of material played a key role for improvement of Li ion diffusion kinetics and electrochemical performances. High temperature impedance studies (EIS) revealed the conductive nature of LNP/C composites in 700 °C 900 °C temperature range. Theoretical particle capacity was found to depend on the particle curvature (i.e., aspect ratio) and highest particle capacity was achieved by a particle of a circular shape.

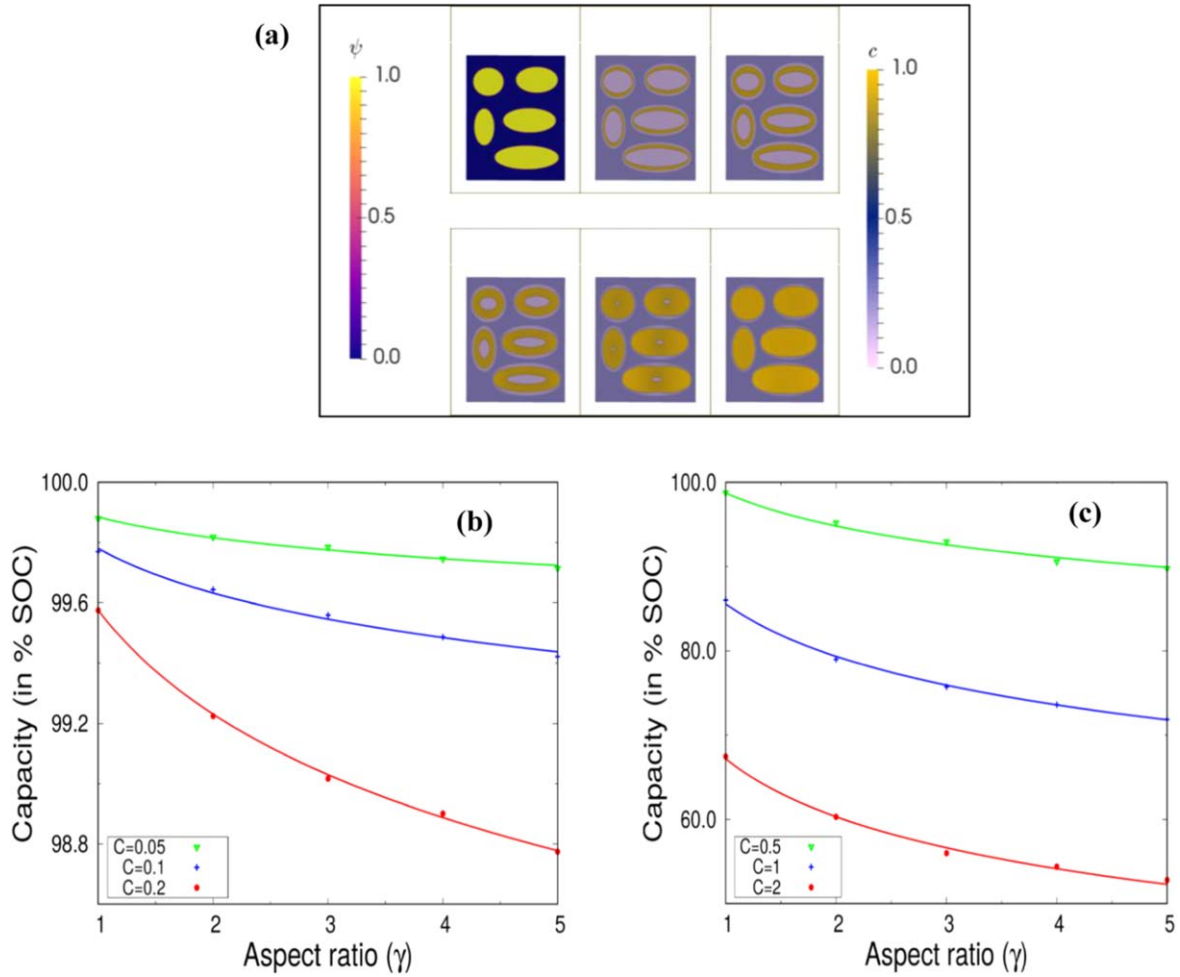

Figure 12. Evolution history of five particles simultaneously (a) The SOC (or duration) values at which phase separation ends at different C rates (b) and (c).

Acknowledgments

Authors acknowledge Quaid i Azam University, Islamabad, Pakistan for the lab facility provision. We are also highly thankful to HEC Pakistan for Project 2014 4768 for Gamry instrument and IRSIP scholarship to Mehwish for accomplishing the battery research at KIT Germany. Institute of Applied Materials (IAM CMS) and Institute for Applied Materials (IAM ESS) Karlsruhe Institute of Technology Germany are highly acknowledged for hosting the scholar for LIBs research. The computational part of this work contributes to the research performed at CELEST (Center for Electrochemical Energy Storage Ulm Karlsruhe) and was partially funded by the German Research Foundation (DFG) under Project ID 390874152 (POLiS Cluster of Excellence). Dr. Ayesha Mujtaba (ayesha.mujtaba@live.com) is acknowledged for EIS discussion.

References

1. M. M. Thackeray, C. Wolverton, and E. D. Isaacs, "Electrical energy storage for transportation—approaching the limits of, and going beyond, lithium-ion batteries." *Energy & Environmental Science*, **5**, 7854 (2012).
2. J. Ni, H. Zhou, J. Chen, and X. Zhang, "LiFePO4 doped with ions prepared by co-precipitation method." *Mater. Lett.*, **59**, 2361 (2005).
3. H.-S. Park, T.-H. Kim, M.-H. Lee, and H.-K. Song, "Catalytic carbonization of an uncarbonizable precursor by transition metals in olivine cathode materials of lithium ion batteries." *J. Mater. Chem.*, **22**, 20305 (2012).
4. J. B. Goodenough and Y. Kim, "Challenges for rechargeable li batteries." *Chem. Mater.*, **22**, 587 (2010).
5. Y. J. Thong, J. H. Beh, J. C. Lai, and T. H. Lim, "Synthesis and characterization of alginate-based sol–gel synthesis of lithium nickel phosphate with surface area control." *Ind. Eng. Chem. Res.*, **58**, 625 (2018).
6. C. Masquelier and L. Croguennec, "Polyanionic (phosphates, silicates, sulfates) frameworks as electrode materials for rechargeable Li (or Na) batteries." *Chem. Rev.*, **113**, 6552 (2013).
7. M. S. Whittingham, "Ultimate limits to intercalation reactions for lithium batteries." *Chem. Rev.*, **114**, 11414 (2014).
8. C. Julien and A. Mauger, "Review of 5-V electrodes for Li-ion batteries: status and trends." *Ionics*, **19**, 951 (2013).
9. Y. Li, J. Wang, H. Huang, J. Wang, M. Zhang, and M. Liang, "Co-coating effect of GdPO4 and carbon on LiFePO4 cathode surface for lithium ion batteries." *Adv. Powder Technol.*, **30**, 1442 (2019).
10. M. Abdollahifar, S.-S. Huang, Y.-H. Lin, Y.-C. Lin, B.-Y. Shih, H.-S. Sheu, Y.-F. Liao, and N.-L. Wu, *High-Performance Carbon-Coated ZnMn2O4 Nanocrystallite Supercapacitors with Tailored Microstructures Enabled by a Novel Solution Combustion Method Journal Power Sources*, **378**, 90 (2018).
11. V. Koleva, R. Stoyanova, and E. Zhecheva, "Nano-crystalline LiMnPO4 prepared by a new phosphate–formate precursor method." *Mater. Chem. Phys.*, **121**, 370 (2010).
12. M. Minakshi, P. Singh, D. Appadoo, and D. E. Martin, "Synthesis and characterization of olivine LiNiPO4 for aqueous rechargeable battery." *Electrochim. Acta*, **56**, 4356 (2011).
13. G. Yang, H. Ni, H. Liu, P. Gao, H. Ji, S. Roy, J. Pinto, and X. Jiang, "The doping effect on the crystal structure and electrochemical properties of LiMnxM1 xPO4 (M = Mg, V, Fe, Co, Gd)." *J. Power Sources*, **196**, 4747 (2011).
14. S. Karthickprabhu, G. Hirankumar, A. Maheswaran, R. D. Bella, and C. Sanjeeviraja, "Structural and electrical studies on Zn2 + doped LiCoPO4." *J. Electrostat.*, **72**, 181 (2014).
15. H. Li, Y. Wang, X. Yang, L. Liu, L. Chen, and J. Wei, "Improved electrochemical performance of 5 V LiCoPO4 cathode materials via yttrium doping." *Solid State Ionics*, **255**, 84 (2014).
16. T. N. L. Doan and I. Taniguchi, "Effect of spray pyrolysis temperature on physical and electrochemical properties of LiCoPO4/C nanocomposites." *Powder Technol.*, **217**, 574 (2012).

17. M. Minakshi, D. Mitchell, R. Jones, F. Alenazey, T. Watcharatharapong, S. Chakraborty, and R. Ahuja, "Synthesis, structural and electrochemical properties of sodium nickel phosphate for energy storage devices." *Nanoscale*, **8**, 11291 (2016).
18. W. Wolfenstine and J. J. Allen, "LiNiPO4–LiCoPO4 solid solutions as cathodes." *J. Power Sources*, **136**, 150 (2004).
19. D. Shanmukaraj and R. Murugan, "Synthesis and characterization of LiNiyCo1 yPO4 (y = 0–1) cathode materials for lithium secondary batteries." *Ionics*, **10**, 88 (2004).
20. F. Yu, L. Zhang, M. Zhu, Y. An, L. Xia, X. Wang, and B. Dai, "Overwhelming microwave irradiation assisted synthesis of olivine-structured LiMPO4 (M = Fe, Mn, Co and Ni) for Li-ion batteries." *Nano Energy*, **3**, 64 (2014).
21. P. R. Kumar, V. Madhusudhanrao, B. Nageswararao, M. Venkateswarlu, and N. Satyanarayana, "Enhanced electrochemical performance of carbon-coated LiMPO4 (M = Co and Ni) nanoparticles as cathodes for high-voltage lithium-ion battery." *J. Solid State Electrochem.*, **20**, 1855 (2016).
22. J. Fan, Y. Yu, Y. Wang, Q.-H. Wu, M. Zheng, and Q. Dong, "Nonaqueous synthesis of nano-sized LiMnPO4@ C as a cathode material for high performance lithium ion batteries." *Electrochim. Acta*, **194**, 52 (2016).
23. V. Borgel, G. Gershinsky, T. Hu, M. G. Theivanayagam, and D. Aurbach, "LiMn0.8Fe0.2PO4/Li4Ti5O12, a possible Li-ion battery system for load-leveling application." *J. Electrochem. Soc.*, **160**, A650 (2013).
24. X. Fuku, K. Kaviyarasu, N. Matinise, and M. Maaza, "Punicalagin green functionalized Cu/Cu2O/ZnO/CuO nanocomposite for potential electrochemical transducer and catalyst." *Nanoscale Res. Lett.*, **11**, 386 (2016).
25. X. G. Mbuyise, E. A. Arbab, K. Kaviyarasu, G. Pellicane, M. Maaza, and G. T. Mola, "Zinc oxide doped single wall carbon nanotubes in hole transport buffer layer." *J. Alloys Compd.*, **706**, 344 (2017).
26. B.-K. Zou, Y. Shao, Z.-Y. Qiang, J.-Y. Liao, Z.-F. Tang, and C.-H. Chen, "LiMPO4 and derived NaMPO4 (Má= áMn, Fe, Mg) with excellent electrochemical properties for lithium/sodium ion batteries." *J. Power Sources*, **336**, 231 (2016).
27. T. Subburaj, Y. N. Jo, K. Prasanna, K. J. Kim, and C. W. Lee, "Titanium oxide nanofibers decorated nickel-rich cathodes as high performance electrodes in lithium ion batteries." *J. Ind. Eng. Chem.*, **51**, 223 (2017).
28. J. Wolfenstine and J. Allen, "Ni3+/Ni2 + redox potential in LiNiPO4." *J. Power Sources*, **142**, 389 (2005).
29. J. Kim, H. Kim, J. Park, and W. Kim, "Large enhancement in mechanical properties of the 6061 Al alloys after a single pressing by ECAP." *Scr. Mater.*, **53**, 1207 (2005).
30. P. S. Herle, B. Ellis, N. Coombs, and L. F. Nazar, "Nano-network electronic conduction in iron and nickel olivine phosphates." *Nat. Mater.*, **3**, 147 (2004).
31. M. Prabu, S. Selvasekarapandian, A. Kulkarni, S. Karthikeyan, G. Hirankumar, and C. Sanjeeviraja, "Structural, dielectric, and conductivity studies of yttrium-doped LiNiPO4 cathode materials." *Ionics*, **17**, 201 (2011).
32. P. R. Kumar, M. Venkateswarlu, M. Misra, A. K. Mohanty, and N. Satyanarayana, "Carbon coated LiMnPO4 nanorods for lithium batteries." *J. Electrochem. Soc.*, **158**, A227 (2011).
33. S. Karthickprabhu, G. Hirankumar, A. Maheswaran, R. D. Bella, and C. Sanjeeviraja, "Influence of metals on the structural, vibrational, and electrical properties of lithium nickel phosphate." *Ionics*, **21**, 345 (2015).
34. L. Vijayan, R. Cheruku, and G. Govindaraj, "Electrical, optical and magnetic investigations on LiNiPO4 based olivines synthesized by solution combustion technique." *Mater. Res. Bull.*, **50**, 341 (2014).
35. A. Örnek, "The synthesis of novel LiNiPO4 core and Co3O4/CoO shell materials by combining them with hard-template and solvothermal routes." *J. Colloid Interface Sci.*, **504**, 468 (2017).
36. A. Örnek, E. Bulut, and M. Can, "Influence of gradual cobalt substitution on lithium nickel phosphate nano-scale composites for high voltage applications." *Mater. Charact.*, **106**, 152 (2015).
37. A. Örnek, "Positive effects of a particular type of microwave-assisted methodology on the electrochemical properties of olivine LiMPO4 (M = Fe, Co and Ni) cathode materials." *Chem. Eng. J.*, **331**, 501 (2018).
38. S. Karthickprabhu, G. Hirankumar, A. Maheswaran, R. Daries Bella, and C. Sanjeeviraja, "Structural, morphological, vibrational and electrical studies on Zn doped nanocrystalline LiNiPO4." *MaterialsScience Forum. 2014. Trans Tech Publ* (2014).
39. L. Dimesso, D. Becker, C. Spanheimer, and W. Jaegermann, "Investigation of graphitic carbon foams/LiNiPO4 composites." *J. Solid State Electrochem.*, **16**, 3791 (2012).
40. K. Rajammal, D. Sivakumar, N. Duraisamy, K. Ramesh, and S. Ramesh, "Influences of sintering temperatures and crystallite sizes on electrochemical properties of LiNiPO4 as cathode materials via sol–gel route for lithium ion batteries." *J. Sol-Gel Sci. Technol.*, **83**, 12 (2017).
41. A. Örnek and M. Z. Kazancioglu, "A novel and effective strategy for producing core–shell LiNiPO4/C cathode material for excellent electrochemical stability using a long-time and low-level microwave approach." *Scr. Mater.*, **122**, 45 (2016).
42. D. Bhuvaneswari, N. Kalaiselvi, N. Jayaprakash, and P. Periasamy, "CAM sol–gel synthesized LiMPO4 (M = Co, Ni) cathodes for rechargeable lithium batteries." *J. Sol-Gel Sci. Technol.*, **49**, 137 (2009).
43. M. Mumtaz, N. K. Janjua, A. Yaqub, and S. Sabahat, "Microwave assisted non-aqueous sol–gel synthesis of LiNiPO4 and its copper doped analogues." *J. Sol-Gel Sci. Technol.*, **72**, 56 (2014).
44. K. Anand, B. Ramamurthy, V. Veeraiah, and K. V. Babu, "Structural, dielectric and conductivity studies of LiNi0.75Mg0.25-xCuxPO4 synthesized by solid state reaction method." *Processing and Application of Ceramics*, **10**, 47 (2016).
45. S. Karthikprabhu, K. Karuppasamy, D. Vikraman, K. Prasanna, T. Maiyalagan, A. Nichelson, A. Kathalingam, and H.-S. Kim, "Electrochemical performances of LiNi1 xMnxPO4 (x = 0.05–0.2) olivine cathode materials for high voltage rechargeable lithium ion batteries." *Appl. Surf. Sci.*, **449**, 435 (2018).
46. K. Anand, B. Ramamurthy, V. Veeraiah, and K. V. Babu, "Effect of magnesium substitution on structural and dielectric properties of LiNiPO4." *Materials Science-Poland*, **35**, 66 (2017).
47. Y. Dong, Y. Zhao, Y. Chen, Z. He, and Q. Kuang, "Optimized carbon-coated LiFePO4 cathode material for lithium-ion batteries." *Mater. Chem. Phys.*, **115**, 245 (2009).
48. B. Wang, A. Abdulla, W. Wang, and D. Zhao, "X., A three-dimensional porous LiFePO4 cathode material modified with a nitrogen-doped graphene aerogel for high-power lithium ion batteries." *Energy & Environmental Science*, **8**, 869 (2015).
49. H.-K. Roh, G.-W. Lee, S. Haghighat-Shishavan, K. Y. Chung, and K.-B. Kim, "Polyol-mediated carbon-coated Li4Ti5O12 nanoparticle/graphene composites with long-term cycling stability for lithium and sodium ion storages." *Chem. Eng. J.*, **385**, 123984 (2020).
50. M. Chen, B. Coasne, D. Derome, and J. Carmeliet, "Coupling of sorption and deformation in soft nanoporous polymers: Molecular simulation and poromechanics." *J. Mech. Phys. Solids*, **137**, 103830 (2020).
51. A. Höweling, A. Stoll, D. O. Schmidt, H. Geßwein, U. Simon, and J. R. Binder, "Influence of synthesis, dopants and cycling conditions on the cycling stability of doped LiNi0.5Mn1.5O4 spinels." *J. Electrochem. Soc.*, **164**, A6349 (2017).
52. L. Wang, Y.-G. Sun, L.-L. Hu, J.-Y. Piao, J. Guo, A. Manthiram, J. Ma, and A.-M. Cao, "Copper-substituted Na0.67Ni0.3 xCuxMn0.7O2 cathode materials for sodium-ion batteries with suppressed P2–O2 phase transition." *Journal of Materials Chemistry A*, **5**, 8752 (2017).
53. X. Cao, X. He, J. Wang, H. Liu, S. Roser, B. R. Rad, and M. Winter, "High voltage LiNi0.5Mn1.5O4/Li4Ti5O12 lithium ion cells at elevated temperatures: carbonate- vs ionic liquid-based electrolytes." *ACS Applied Materials & Interfaces*, **8**, 25971 (2016).
54. V. Nilsson, A. Kotronia, M. Lacey, K. Edstrom, and P. Johansson, "Highly concentrated LiTFSI–EC electrolytes for lithium metal batteries." *ACS Appl. Energy Mater.*, **3**, 200 (2019).
55. V. Sharova, A. Moretti, T. Diemant, A. Varzi, R. J. Behm, and S. Passerini, "Comparative study of imide-based Li salts as electrolyte additives for Li-ion batteries." *J. Power Sources*, **375**, 43 (2018).
56. L. Wang, Y.-G. Sun, L.-L. Hu, J.-Y. Piao, J. Guo, A. Manthiram, J. Ma, and A. M. Cao, "Copper-substituted Na0.67 Ni 0.3 x Cu x Mn 0.7 O 2 cathode materials for sodium- ion batteries with suppressed P2–O2 phase transition." *Journal of Materials Chemistry A*, **5**, 8752 (2017).
57. Y. Zhang, Y. Pan, J. Liu, G. Wang, and D. Cao, "Synthesis and electrochemical studies of carbon-modified LiNiPO 4 as the cathode material of Li-ion batteries." *Chem. Res. Chin. Univ.*, **31**, 117 (2015).
58. G. Ning, B. Haran, and B. N. Popov, "Capacity fade study of lithium-ion batteries cycled at high discharge rates." *J. Power Sources*, **117**, 160 (2003).
59. P. Zou, Z. Lin, M. Fan, F. Wang, Y. Liu, and X. Xiong, "Facile and efficient fabrication of Li3PO4-coated Ni-rich cathode for high-performance lithium-ion battery." *Appl. Surf. Sci.*, **504**, 144506 (2020).
60. S. Lim, W. Ryu, W. Kim, and H. Kwon, "of LiNi0.5Mn1Electrochemical performance .5O4 cathode material fabricated from nanothorn sphere structured MnO2." *ECS Symp Abstr*, 953 (2012).
61. S. B. R. S. Adnan, N. S. Mohamed, N. A. Mustaffa, N. Zainal, S. Ibrahim, and Z. Radzi, "Thermal, structural and electrical properties of Li2BaSiO4 ceramic electrolyte." *Ceramic International*, **45**, 1424 (2019).
62. M. Afzal, M. Saleemi, B. Wang, C. Xia, W. Zhang, Y. He, and B. Zhu, "Fabrication of novel electrolyte-layer free fuel cell with semi-ionic conductor (Ba0. 5Sr0. 5Co0. 8Fe0. 2O3 δ-Sm0. 2Ce0. 8O1. 9) and Schottky barrier." *J. Power Sources*, **328**, 136 (2016).
63. A. A. Jais, S. M. Ali, M. Anwar, M. R. Somalu, A. Muchtar, W. N. R. W. Isahak, and N. P. Brandon, "Enhanced ionic conductivity of scandia-ceria-stabilized-zirconia (10Sc1CeSZ) electrolyte synthesized by the microwave-assisted glycine nitrate process." *Ceram. Int.*, **43**, 8119 (2017).
64. B. A. Mei, O. Munteshari, J. Lau, B. Dunn, and L. Pilon, "Physical interpretations of Nyquist plots for EDLC electrodes and devices." *The Journal of Physical Chemistry C*, **122**, 194 (2018).
65. J. P. Sabawa and A. S. Bandarenka, "Degradation mechanisms in polymer electrolyte membrane fuel cells caused by freeze-cycles: Investigation using electrochemical impedance spectroscopy." *Electrochim. Acta*, **311**, 21 (2019).
66. J. Cao, Y. Qu, and R. Guo, "La0. 6Sr0. 4CoO3 δ modified LiFePO4/C composite cathodes with improved electrochemical performances." *Electrochim. Acta*, **67**, 152 (2012).
67. S. Karthickprabhu, G. Hirankumar, A. Maheswaran, C. Sanjeeviraja, and R. D. Bella, "Structural and conductivity studies on LiNiPO4 synthesized by the polyol method." *J. Alloys Compd.*, **548**, 65 (2013).
68. J. Taracson and M. Armand, "Issues and challenges facing lithium ion batteries." *Nature*, **414**, 359 (2001).
69. D. K. Kim, P. Muralidharan, H.-W. Lee, R. Ruffo, Y. Yang, C. K. Chan, H. Peng, R. A. Huggins, and Y. Cui, "Spinel LiMn2O4 nanorods as lithium ion battery cathodes." *Nano Lett.*, **8**, 3948 (2008).

70. J. Vetter, P. Novák, M. R. Wagner, C. Veit, K.-C. Möller, J. Besenhard, M. Winter, M. Wohlfahrt-Mehrens, C. Vogler, and A. Hammouche, "Ageing mechanisms in lithium-ion batteries." *J. Power Sources*, **147**, 269 (2005).
71. M. S. Whittingham, "Lithium batteries and cathode materials." *Chem. Rev.*, **104**, 4271 (2004).
72. C. Liu, F. Li, L. P. Ma, and H. M. Cheng, "Advanced materials for energy storage." *Adv. Mater.*, **22**, E28 (2010).
73. J. Santoki, D. Schneider, M. Selzer, F. Wang, M. Kamlah, and B. Nestler, "Phase-field study of surface irregularities of a cathode particle during intercalation." *Modell. Simul. Mater. Sci. Eng.*, **26**, 065013 (2018).
74. C. V. Di Leo, E. Rejovitzky, L. Anand, and A. Cahn–Hilliard-type, "Phase-field theory for species diffusion coupled with large elastic deformations: application to phase-separating Li-ion electrode materials." *J. Mech. Phys. Solids*, **70**, 1 (2014).
75. P. Stein, Y. Zhao, and B.-X. Xu, "Effects of surface tension and electrochemical reactions in Li-ion battery electrode nanoparticles." *J. Power Sources*, **332**, 154 (2016).
76. Z. Guo, L. Ji, and L. Chen, "Analytical solutions and numerical simulations of diffusion-induced stresses and concentration distributions in porous electrodes with particles of different size and shape." *J. Mater. Sci.*, **52**, 13606 (2017).